ELSEVIER

Journal of Neuroscience Methods 94 (1999) 93–103

JOURNAL OF NEUROSCIENCE METHODS

www.elsevier.com/locate/jneumeth

Using partial directed coherence to describe neuronal ensemble interactions

Koichi Sameshima [a,*], Luiz Antonio Baccalá [b]

[a] *Discipline of Medical Informatics and Laboratory of Functional Neurosurgery, School of Medicine, University of São Paulo, Av. Dr Arnaldo 455, CEP 01246-903 São Paulo, SP, Brazil*

[b] *Department of Telecommunications and Controls, Escola Politécnica, University of São Paulo, São Paulo, Brazil*

Received 30 June 1999; accepted 6 August 1999

Abstract

This paper illustrates the use of the recently introduced method of *partial directed coherence* in approaching how interactions among neural structures change over short time spans that characterize well defined behavioral states. Central to the method is its use of multivariate time series modelling in conjunction with the concept of Granger causality. Simulated neural network models were used to illustrate the technique's power and limitations when dealing with neural spiking data. This was followed by the analysis of multi-unit activity data illustrating dynamical change in the interaction of thalamo-cortical structures in a behaving rat.

Keywords: Partial directed coherence; Granger causality; Structural inference; Feedback detection; Spike train analysis; Multivariate autoregressive models

1. Introduction

Evidence is mounting that challenges the traditional view of the brain as a set of segregated tissues with static specialized functions. While neural plastic changes in adult brains over days or weeks are well documented (Merzenich et al., 1981; Recanzone et al., 1992; Donoghue, 1995; Wang et al., 1995; Nudo et al., 1997), the neural dynamics involved in the genesis of animal behavior over short time scales is only now being more deeply investigated (Calford and Tweedale, 1991; Nicolelis et al., 1993; Faggin et al., 1997; Schreiner et al., 1997). It is thought that these dynamics stems from the parallel and synchronized activity of many neurons and that its understanding requires monitoring large ensembles of neuronal populations simultaneously (Eichenbaum and Davis, 1998; Nicolelis, 1998).

To organize specific behavior neural structures may interact directly or indirectly and their effective functional instantaneous connection may possibly be switching and varying in strength over short time spans. In describing these functional interactions, most researchers select pairs of functional elements and subject their activity to cross-correlation and spectral (coherence) analysis (Gochin et al., 1991; Duckrow and Spencer, 1992; Bressler et al., 1993; Konig et al., 1995). Though intuitive and powerful, reliable use of these tools requires neural data segments longer than the time scales characterizing stationary animal behavior thus producing, at best, only greatly averaged estimates with poor temporal resolution (Perkel et al., 1967; Aertsen and Gerstein, 1985; Eggermont, 1990). In addition, pairwise correlations and spectral coherence only examine if some link exists between two neural elements and do not address whether one structure drives the other or if there is feedback between those structures.

This latter limitation for bivariate time series was overcome by Saito and Harashima's (Saito and Harashima, 1981) method of *directed coherence* (Schnider et al., 1989; Baccalá and Sameshima, 1998; Baccalá et al., 1998), which represents a factorization of spectral coherence (via time series modelling) (Baccalá and Sameshima, 1999). Perhaps more importantly, this technique relies on the key concept of Granger causality

* Corresponding author.
E-mail address: ksameshi@usp.br (K. Sameshima)

0165-0270/99/$ - see front matter
PII: S0165-0270(99)00128-4

(Granger, 1969) between time series (named after its proponent to distinguish it from other causality concepts in other fields): *an observed time series x(n) Granger-causes another series y(n), if knowledge of x(n)'s past significantly improves prediction of y(n); this relation between time series is not reciprocal, i.e. x(n) may Granger-cause y(n) without y(n) necessarily Granger-causing x(n).* This lack of reciprocity permits gauging the direction of information flow between structures and allows probing for feedback which exists

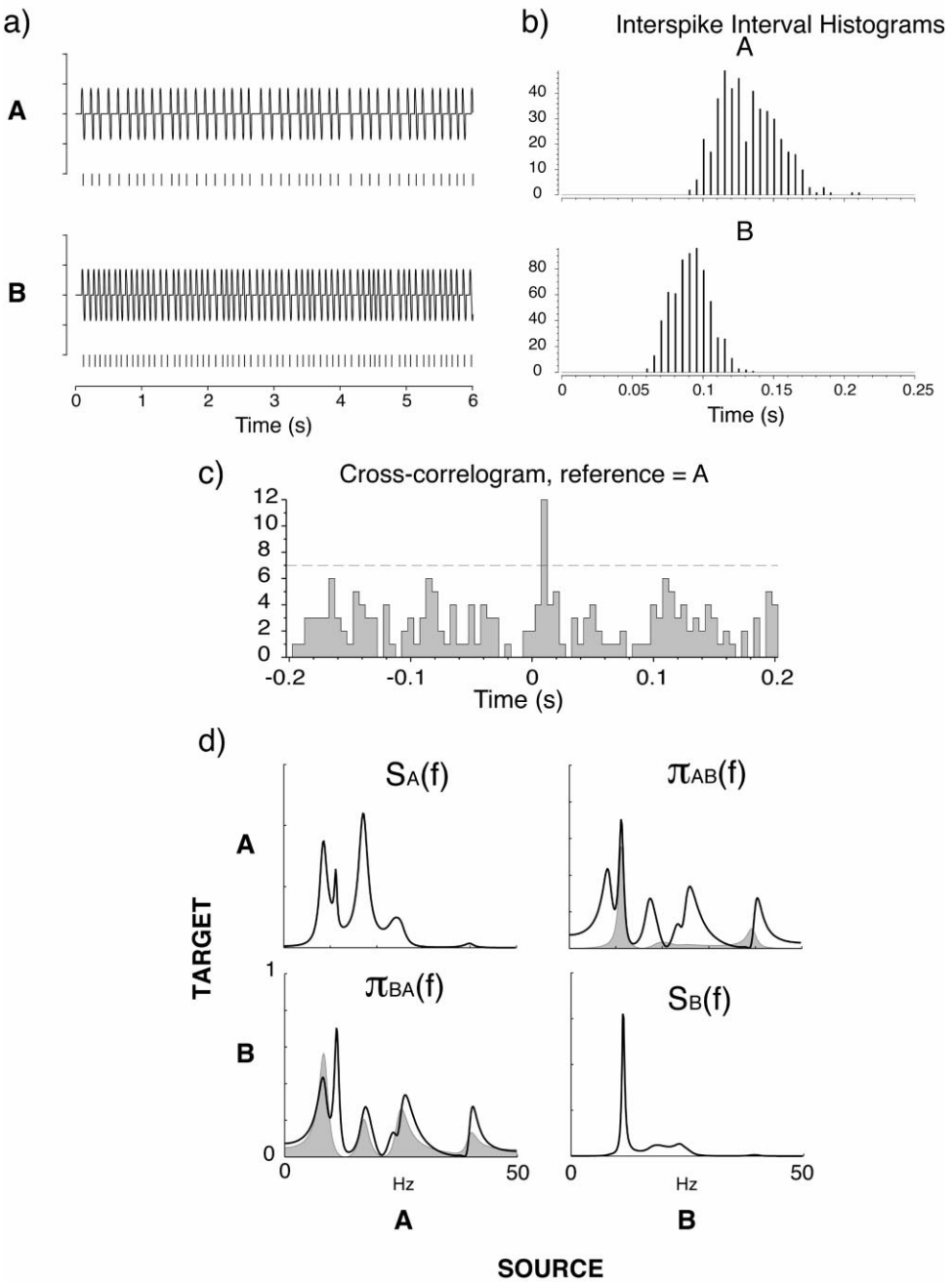

Fig. 1. (a) An example of 6 s of spike time-stamps and kernel reconstructed signals from neurons A and B under scenario I of Example 1. (b) The respective ISI histograms showing distinct average firing rates that is also reflected in the oscillatory power spectra $S_A(f)$ and $S_B(f)$ in (d). (c) Cross-correlation histogram (5 ms binwidth) between neurons A (45 spikes) and B (65 spikes) shows a significant peak at 10 ms lag reflecting the excitatory connection from A to B. The horizontal dashed-line is $>99\%$ confidence limits supposing Poisson processes. (d) The mutual interneuronal influence is shown by the partial directed coherences $\pi_{BA}(f)$ and $\pi_{AB}(f)$ (shaded areas). Significant causality was observed for both connections as $\pi_{BA}(f)$ and $\pi_{AB}(f)$ rise above the significance (dotted line) adopted for the SCC criterion (see Remark 2). Note that $\pi_{BA}(f)$ and $\pi_{AB}(f)$ achieve significant levels at distinct frequencies. The observed presence of causality from A to B and from B to A is in accord with existing feedback underlying scenario I, that can not be inferred from the cross-correlogram (c). The solid lines on the $\pi_{ij}(f)$ graphs depict the existing classical coherence ($C_{AB}(f) = C_{BA}(f)$) between A and B.

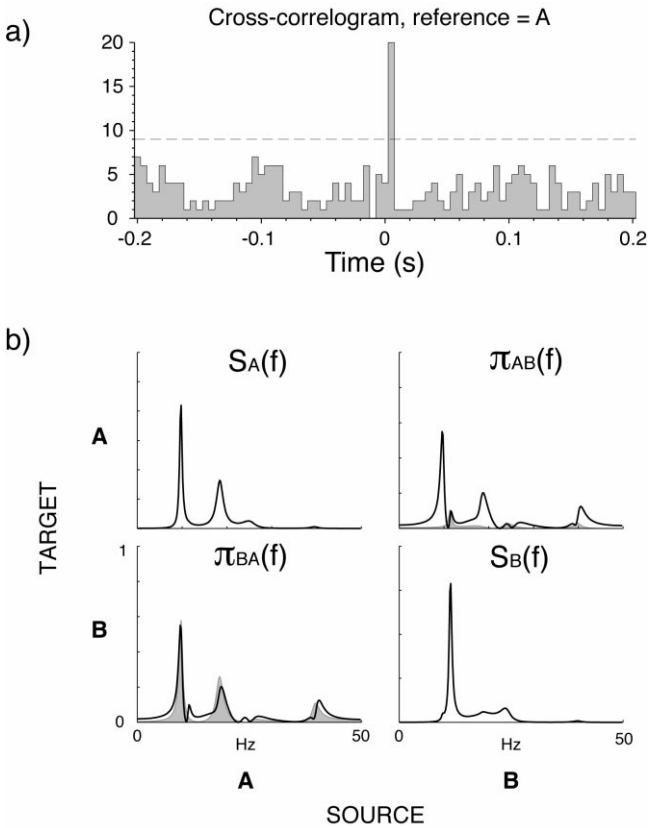

Fig. 2. Six seconds of simulation results for scenario II of Example 1 (unidirectional connection from A to B, with 59 and 69 spikes, respectively) of (a) the cross-correlation histogram (5 ms binwidth) showing that A leads B by 5 ms, and (b) where only the partial directed coherence $\pi_{BA}(f)$ is above the dotted significance line for SCC (Remark 2) in accord with the unidirectional character of the connection from A to B. The shaded area of $\pi_{BA}(f)$ has the classical coherence $C_{BA}(f)$ $(=C_{AB}(f))$ as its envelope (solid line); in other words, in this case all of existent synchronous activity is due to neuron A.

whenever one can show that $x(n)$ Granger-causes $y(n)$, and $y(n)$ simultaneously Granger-causes $x(n)$.

In a recent paper (Baccalá et al., 1998), we discussed the use of Granger causality and directed coherence in the analysis of multivariate measurements of local field potentials, and provided a specific test of the presence of causal relationships. In this paper, we investigate the performance of the recently introduced frequency domain method of partial directed coherence (Baccalá and Sameshima, 1999) to the analysis of dynamic changes in the connections among neural structures in a spike train data context. For comparisons, we also included the results of a Granger causality test (GCT) discussed in Baccalá et al. (1998).

2. Causality determination and multivariate autoregressive models

To use multivariate time series techniques we first preprocessed the neural spiking data (labelled via their time stamps t_k) prior to analysis, by convolving the spike impulse trains

$$s_i(t) = \sum_k \delta(t - t_k)$$

with the kernel

$$h(t) = \frac{\sin(\pi t/T_w)}{\pi t/T_w} \tag{2.1}$$

and by sampling the result at a rate $1/T_s$, leading to discrete time signals $x_i(n)$, $1 \le i \le N$, after extraction of their means (French and Holden, 1971). To describe the mutual relations between $x_i(n)$ we employed a multivariate (vector) autoregressive model (Priestley, 1981; Lutkepohl, 1993):

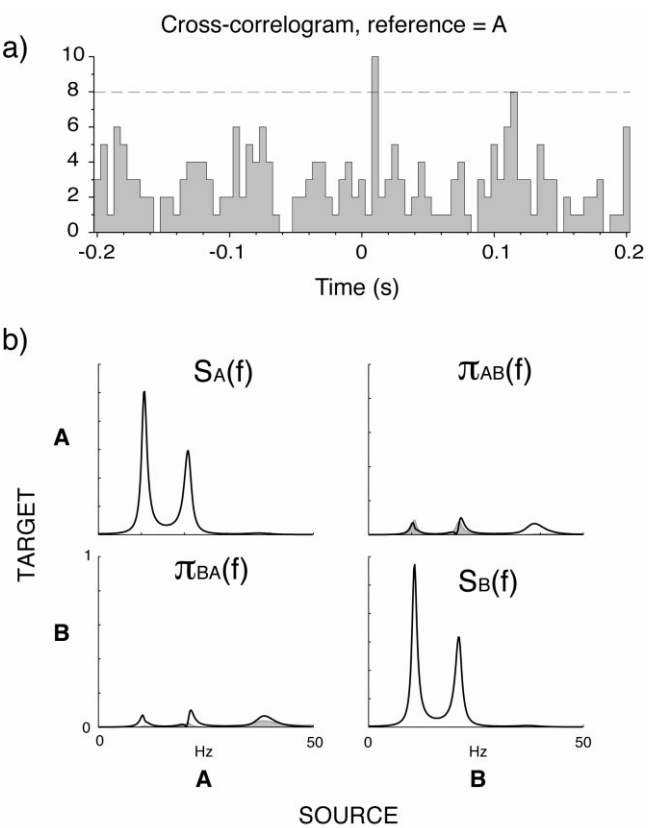

Fig. 3. (a) The spike cross-correlogram (binwidth = 5 ms) using 6 s of a simulation realization (with 58 and 59 spikes) under scenario III (Example 1), with a significant peak at 10 ms lag. In (b), the partial directed coherences $\pi_{BA}(f)$ and $\pi_{AB}(f)$ stay below the dotted significance line above for SCC (Remark 2) in agreement with the unconnected nature of the pair of neurons. The classical coherences $C_{AB}(f) = C_{BA}(f)$ between A and B are also shown (solid line) on the same graphs. Note that the cross-correlogram (a) for 6 s segment falsely suggests the presence of connection.

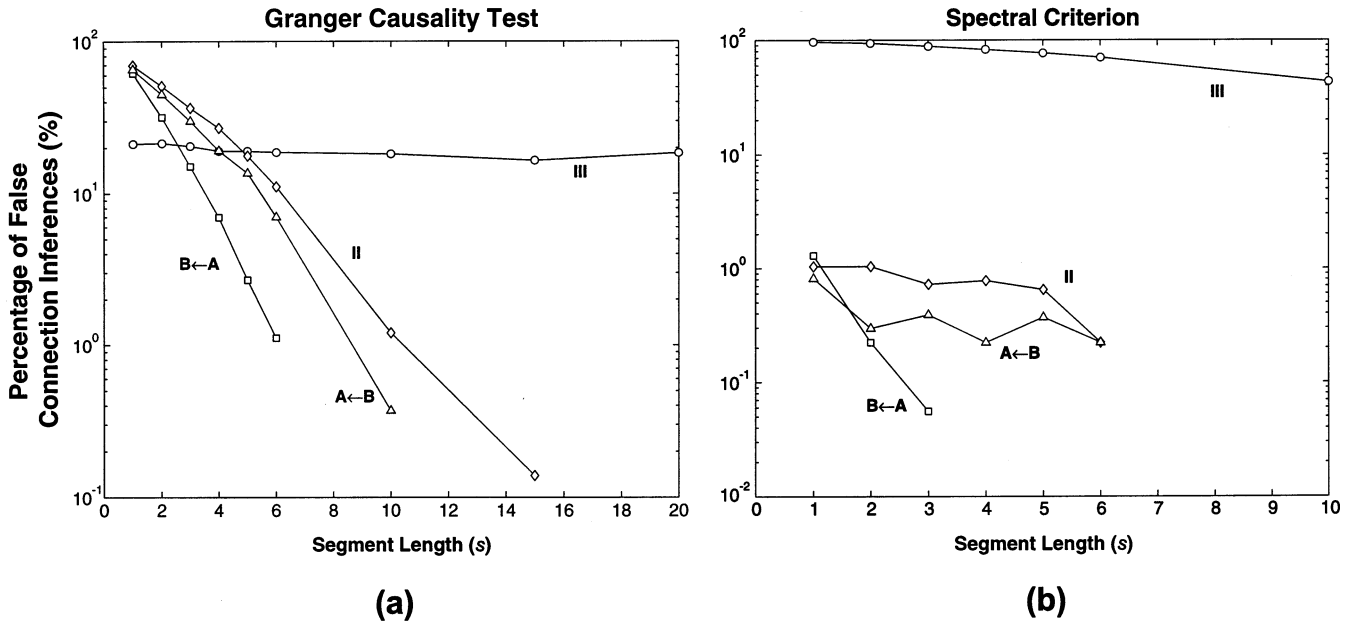

Fig. 4. Percentage of false structural inferences of Example 1 using the Granger causality test (a) and the spectral causality criterion (b). For scenario I, results are broken into false inferences respectively for connections from A to B (B←A) and from B to A (A←B). For scenario II, only the results of its existing connection from A to B are shown together with the results for scenario III that lacks connections. Better performance arises for actually present connections with superior performance for the spectral criterion. For absent connections (scenario III), the Granger test structure inference failure remained at 20% irrespective of signal duration, while the spectral criterion failure rate, though higher, decreased as signal duration increased. For existing connections, inference errors around 1% for 1–2 s long segment were attained for the spectral criterion illustrating its high temporal resolution.

$$\begin{bmatrix} x_1(n) \\ \vdots \\ x_N(n) \end{bmatrix} = \sum_{r=1}^{p} \mathbf{A}_r \begin{bmatrix} x_1(n-r) \\ \vdots \\ x_N(n-r) \end{bmatrix} + \begin{bmatrix} w_1(n) \\ \vdots \\ w_N(n) \end{bmatrix} \tag{2.2}$$

with $w_i(n)$ standing for white uncorrelated innovations noises. To determine the prediction coefficient matrices A_r for each lag r, we employed standard fast maximum entropy methods, and to choose the appropriate order of the model p we used Akaike's *AIC* criterion (Marple Jr, 1987). The time domain representation of Eq. (2.2) is easily translated into the frequency domain by computing the power spectral density matrix (Priestley, 1981)

$$\mathbf{S}(f) = \mathbf{H}(f)\Sigma\mathbf{H}(f)^H, \tag{2.3}$$

where Σ is a covariance matrix of $w_i(n)$,

$$\mathbf{H}(f) = \bar{\mathbf{A}}^{-1}(f) = (\mathbf{I} - \mathbf{A}(f))^{-1} \tag{2.4}$$

and $\mathbf{A}(f) = \Sigma_{r=1}^{p} \mathbf{A}_r z^{-r}\big|_{z=e^{-j2\pi f}}$. Let $a_{ij}(r)$ be an element of A_r. Also let $\bar{a}_{ij}(f)$ be $\bar{A}$'s i, j-th element, i.e. the i-th component of the j-th column $\bar{\mathbf{a}}_j(f)$ of $\bar{A}$.

Partial directed coherence was introduced recently as a modification/generalization (Baccalá and Sameshima, 1999) of directed coherence (Saito and Harashima, 1981; Schnider et al., 1989; Baccalá and Sameshima, 1998; Baccalá et al., 1998) and its variant — the method of '*directed transfer function*' (Kaminski and Blinowska, 1991). The main reason for introducing partial directed coherence is that it provides a clearer and more immediate frequency domain connectivity picture of Granger causality than that due to directed coherence (Baccalá and Sameshima, 1999), especially for the simultaneous analysis of more than two time series ($N > 2$).

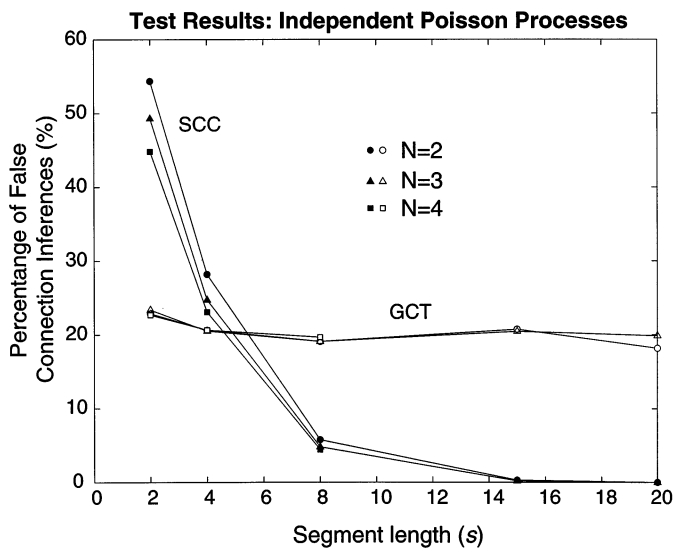

Fig. 5. Percentage of false structural inferences of independent simultaneously processed Poisson processes ($N = 2$, 3 and 4) for increasing segment lengths using the Granger causality test (a) and the spectral causality criterion (b). The kernel convolution parameters used were $T_w = 50$ ms and $1/T_s = 200$ Hz.

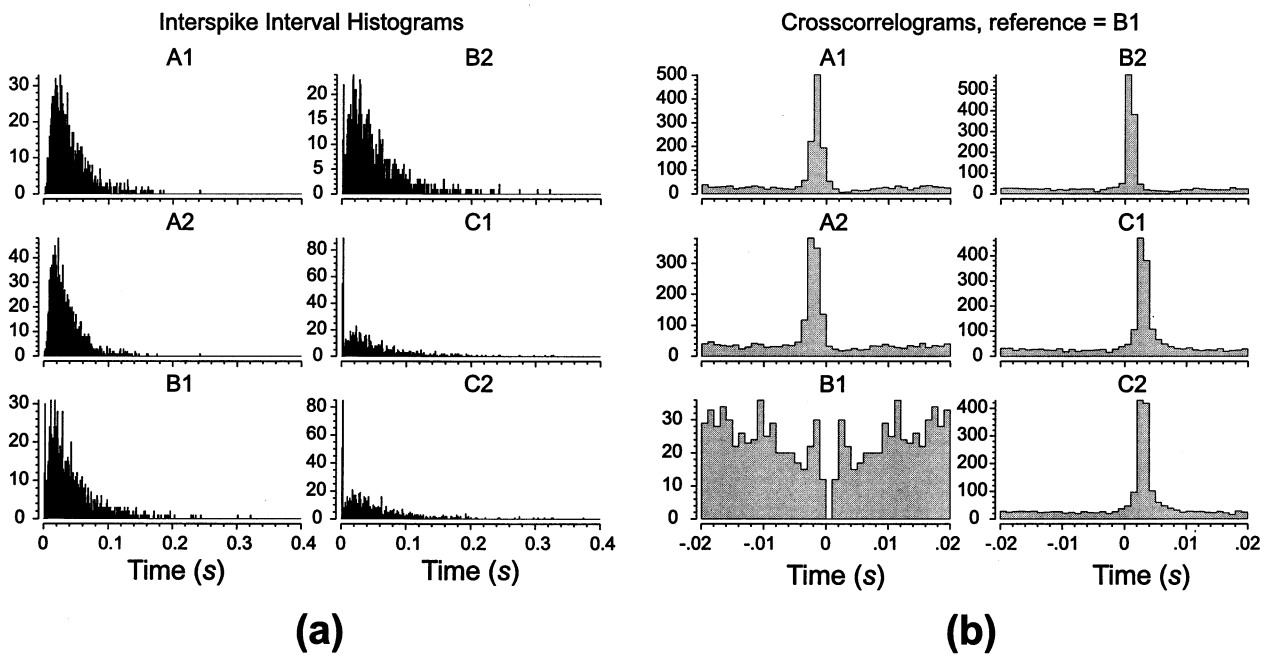

Fig. 6. (a) Sample of inter-spike interval histograms for two neurons from each layer (40 s of simulation) of Example 2 where layer B and C neurons show bursting ISI patterns and where (b) cross-correlograms using B1 neuron as reference (binwidth = 1 ms) point to a propagation latency of about 2 ms between layers.

Testing for Granger causality from series j to i, i.e. probing for the improvements in predicting series i from past observations of series j actually depends on asserting whether $a_{ij}(r) = 0$ for all lags (Lutkepohl, 1993; Baccalá et al., 1998). The frequency domain equivalent of this concept is $\bar{a}_{ij}(f) = 0$ for all f. Thus. after suitable normalization, discussed elsewhere (Baccalá and Sameshima, 1999), one possible definition for '*partial directed coherence*' is

$$\pi_{ij}(f) \stackrel{\Delta}{=} \frac{\bar{a}_{ij}(f)}{\sqrt{\bar{\mathbf{a}}_j(f)^H \bar{\mathbf{a}}_j(f)}} \tag{2.5}$$

Remark 1: This name, '*partial directed coherence*', follows from another possible normalization (Baccalá and Sameshima, 1999) of $\bar{a}_{ij}(f)$ whereby the resulting $\pi_{ij}(f)$ is a natural factor term in the partial coherence $\kappa_{ij}(f)$ between two time series (Bendat and Piersol, 1986). By itself $\kappa_{ij}(f)$ describes the linear pairwise time series relatedness (without reference to the direction of information flow) after discounting the common effect due to other simultaneously observed series.

Remark 2: When $N = 2$, the method of '*partial directed coherence*' leads exactly to the same estimator as the method of '*directed transfer function*' (Kaminski and Blinowska, 1991). This identity authorizes the use of an empirical spectral causality criterion (SCC) suggested by Schnider et al. (1989) whereby connection from j to i is significant if $|\pi_{ij}(f)| > 0.1$, for some f. Since multivariate series decomposition into partial directed coherences effectively separates pairwise interactions by subtracting the effect of other series, we tentatively adopted SCC also for $N > 2$.

Remark 3: The main advantage of partial directed coherence is that Granger causality may be assessed over specific frequency ranges as opposed to GCT which considers the spectrum as a whole.

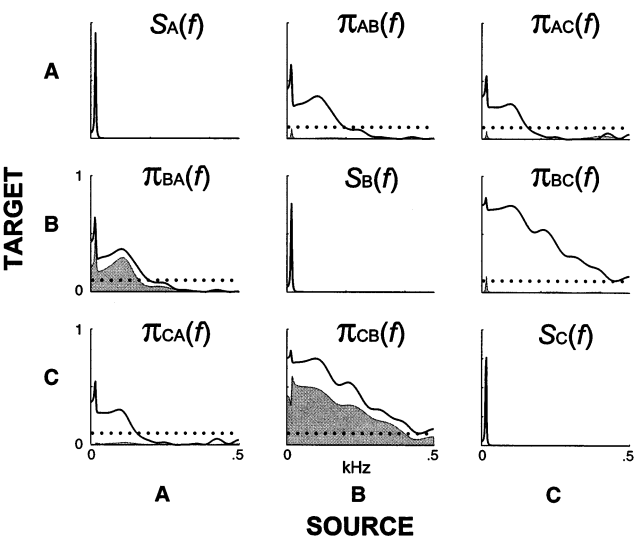

Fig. 7. Three-by-three matrix subplot layout containing the power spectral densities, $S_i(f)$, of simultaneously analyzed neurons along the main diagonal, one from each layer of Example 2; the respective partial directed coherences lie on the off-diagonal subplots, where only $\pi_{BA}(f)$ and $\pi_{CB}(f)$ (shaded) are significantly larger than 0.1 (dotted line) in accord with the simulated layer structure (A → B → C). Classical coherence plots (solid line) are significant throughout the network. This further illustrates $C_{ij}(f)$'s inability to provide detailed structural information.

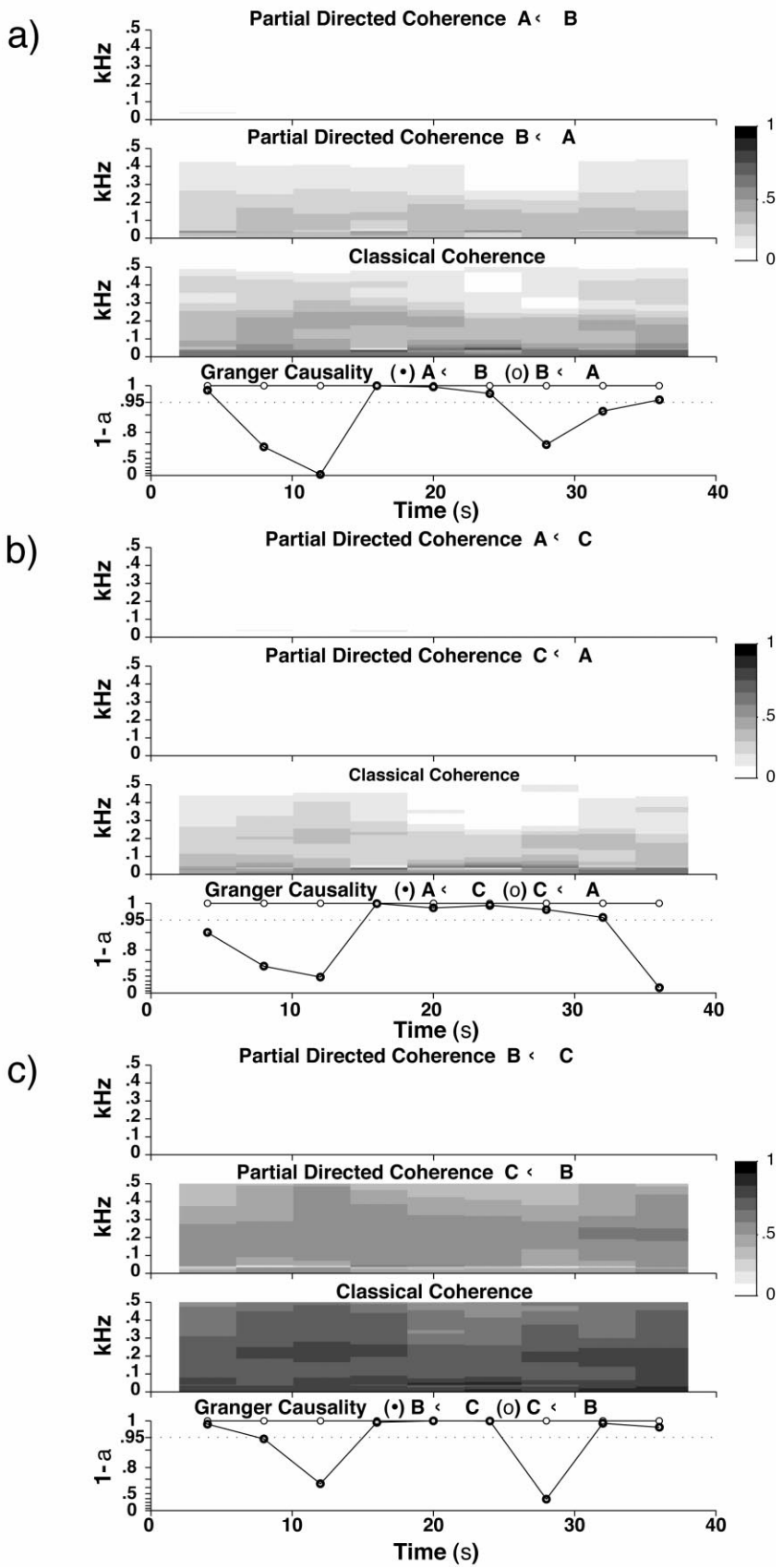

Fig. 8. Time-frequency representation of causality obtained by collating coherence estimates (in 10 level grey scale) for adjacent 8 s long segments (50% overlapping) with four plots for each time series pair showing that (a) $\pi_{AB}(f) \simeq 0$ as opposed to persistently significant $\pi_{BA}(f)$ as confirmed by the Granger causality test (a plot of the $1-\alpha = 95\%$ confidence level) where information flows from A to B (○) with some false positive connectivity results in the opposite direction (●); (b) lack of direct connection between A and C ($\pi_{AC}(f) \simeq \pi_{CA}(f) \simeq 0$) with mostly wrong Granger test results and (c) $\pi_{BC}(f) \simeq 0$ and significant $\pi_{CB}(f)$ with the Granger test behaving as in (a). Together these figures confirm the overall structure $A \rightarrow B \rightarrow C$ according the spectral criterion (see Remark 2).

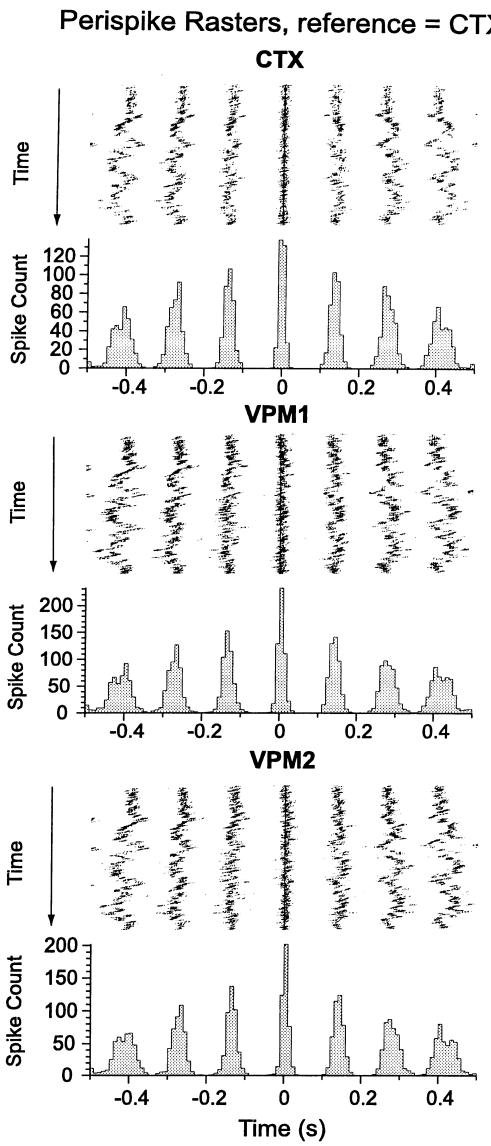

Fig. 9. Perispike raster plots and cross-correlograms (10 ms binwidth), using cortical (CTX) activity as reference, of a simultaneous multi-unit thalamo-cortical recording of rhythmic spike train bursting at 7.4 Hz over 20 s. Note the nonstationary frequency fluctuations possibly reflecting changes in the animal's internal state. The cross-correlograms reveal that on average cortical activity (CTX) leads thalamic bursting (VPM1 and VPM2) suggesting predominant cortical driving of thalamic neurons.

For comparisons, we used classical coherence (Bendat and Piersol, 1986) for series pairs i and j, which were computed via

$$C_{ij}(f) = \frac{|\hat{S}_{x_i x_j}(f)|^2}{\hat{S}_{x_i}(f)\hat{S}_{x_j}(f)} \tag{2.6}$$

where $\hat{S}_{x_i}(f)$ and $\hat{S}_{x_i x_j}(f)$ stand for estimates of the series auto- and cross-spectrum obtained through Eq. (2.3). High $C_{ij}(f)$ values point to the simultaneous activation (degree of relative synchrony) between areas i and j at frequency f and to the adequacy of describing their existing interaction through a linear operator in that frequency range.

3. Illustrative examples

3.1. Example 1: Two neuron integrate-and-fire network

To illustrate causality analysis in a neural spiking context, we simulated a simple two neuron integrate-and-fire network. Each neuron was implemented by a discrete time summation of its past input leading to an internal potential (V_m) that was reset to zero and produced a spike of unit amplitude in normalized units whenever a threshold value (V_{th}) was reached and the neuron was outside its refractory period (R). In the simulations, independent white uniform noise between 0 and 1 at the inputs of each neuron simulated a stochastic background. These neurons interacted by adding their weighted (k_i) output after some propagation delay to the respective input of the other neuron. Using identical neurons ($V_{th} = 10$ in normalized units and $R = 50$ ms) we obtained oscillatory behavior around 10 Hz when neurons were unconnected.

The resulting simulations (90 Monte Carlo experiments each lasting 60 s) of spike stamps for both neurons were processed via Eq. (2.1) using $T_w = 5$ ms and $1/T_s = 100$ Hz before modelling via Eq. (2.2) wherefrom we computed the partial directed coherence to compare a test for Granger causality with the spectral causality criterion in the scenarios of:

1. bi-directional connectivity, one excitatory connection from neuron A to neuron B and a reverse inhibitory connection of identical strength from B to A, (i.e. $k_A = -k_B = 2$);
2. unidirectional connection from A to B ($k_A = 2$, $k_B = 0$), and
3. absent connection ($k_A = 0$, $k_B = 0$).

A 6 s segment of spike time stamps and the corresponding $x_A(n)$ and $x_B(n)$ for scenario I are shown in Fig. 1a followed by inter-spike interval (ISI) histograms (Fig. 1b) and spike cross-correlation (Fig. 1c). Partial directed coherence analysis (shaded areas in Fig. 1d) confirmed the existing bi-directional influence. Note how driving due to different neurons predominated at different frequencies. This kind of frequency dependent feedback from B to A was impossible to infer either from spike cross-correlation or from the existing fairly high ordinary coherence $C_{AB}(f) = C_{BA}(f)$. In fact, high $C_{AB}(f)$ meant that there was significant synchronous co-activation without additional information as to the which neuron was the predominant driving source at which frequency.

In an example of a 6 s long segment for scenario II, the cross-correlation (Fig. 2a) was contrasted to the partial directed coherence (Fig. 2b). The small value of

$\pi_{AB}(f)$ correctly confirmed absence of feedback from B to A. Such deduction was impossible using cross-correlation.

The cross-correlation (Fig. 3a) for an example of a 6 second long segment of scenario III incorrectly led to the inference of an existing connection. Correct inference confirming lack of connection was achieved using partial directed coherence (Fig. 3b).

The percentage of false structural inferences for GCT (Fig. 4a) and SCC (Fig. 4b) as a function of segment length showed SCC's superiority when connections were present: achieving the highest temporal resolution for 1–2% failure for segments as short as 1–2 s. For unconnected neurons both tests produced high failure rates, 20% for GCT, irrespective of segment length, and high, but declining, SCC failure for increasing segment length.

To further evaluate SCC's failure rate for identical unconnected neurons, we investigated test performance by simultaneously analyzing 2, 3 and 4 independent Poisson processes firing around 10 Hz (45 realizations each lasting 120 s) (Fig. 5). In this case, SCC's performance was superior to GCT's which behaved as before. SCC detected lack of connection correctly for as few as 80 observed spikes (8 s segments) in most cases.

3.2. Example 2: Multi-layered multi-neuronal model simulation

To investigate causality that was due to neuronal bursting behavior, we simulated the interaction of many leaky integrate-and-fire neurons disposed in three layers using the cortical cell parameters from Wehmeier et al. (1989).

The model layers (with unidirectional feedforward interconnection among them: $A \rightarrow B \rightarrow C$) contained 50 neuronal elements each, all identical but for randomly chosen thresholds between -45 to -35 mV. Each neuron in A was connected to all neurons in B, each of whose neurons projected to all neurons in C; with 10% inhibitory synaptic inputs driven by Poisson processes with $\lambda = 0.01$. The propagation delay between layers was 2 ms. We employed backward-Euler integration with $T_{step} = 0.0001$ s; and discarded the initial transient to avoid nonstationarity in the analysis. Within layer B or C, each neuronal element received exactly the same input stimulus set from the previous layer; while a random Poisson process acted on layer A neurons.

Prior to analysis, the spike trains resulting from the simulation were convolved with Eq. (2.1) using $T_w = 50$ ms and $1/T_s = 1$ kHz. Sample ISI histograms for two neurons from each layer are displayed in Fig. 6a (40 s of simulation); layer B and C neurons show bursting ISI histograms patterns. Neurons in A fired between 24.9 and 29.5 Hz, while B and C layer neurons averaged respectively 24.2 and 20.9 Hz firing. Cross-correlograms between A, B and C, shown in Fig. 6b, pointed to a propagation latency of approximately 2 ms between layers.

Using 8 seconds of three neurons, one of each layer, we displayed the series' power spectra along the main diagonal of the 3×3 subplot result matrix layout of Fig. 7; the off-diagonal layout plots exhibit partial directed coherence (shaded) and classical coherence (solid line). The direct influence of neuron A over neuron B via their partial directed coherences $\pi_{BA}(f)$ was significant as was that from B to C ($\pi_{CB}(f)$) in contrast to all other directional pairs that showed negligible partial directed coherence confirming unequivocally the information flow diagram: $A \rightarrow B \rightarrow C$.

To follow changes in the information flow pattern we produced a time-frequency representation by collating coherence estimates (gray scale) for adjacent 8 s long segments (with 50% overlapping among adjacent segments) in Fig. 8. For each pair of time series, four plots were displayed: the two partial directed coherences; the classical coherence; and the Granger causality test (see the Appendix of Baccalá et al. (1998)). Fig. 8a shows how neurons in A and B interact: a) $\pi_{AB}(f) \simeq 0$ throughout, as opposed to persistently significant $|\pi_{BA}(f)| > 0.1$; b) classical coherence reflected the correlated activity of both neurons; c) the Granger causality test confirmed the connectivity from A to B (o), but yielded some false positive connectivity from B to A in accord with the results in Fig. 4 and 5. The lack of direct connection between A and C was reflected in the partial directed coherence results of Fig. 8b though GCT incorrectly signalled the existence of this connection as being direct. The results in Fig. 8c, for B and C, were qualitatively similar to those in Fig. 8a.

3.3. Example 3: Analysis of measured spike sequences

Finally, we analyzed thalamo-cortical data of a rat engaged in exploratory activity. Using a simultaneous multi-unit recording without individual spike discrimination, multiple neuron spike trains with rhythmic bursting around 7.4 Hz were studied. Perispike raster plots (Fig. 9), using cortical (CTX) activity as reference, showed that the oscillation frequency varied over a 20 s span possibly due to non-stationary fluctuations in the animal's internal state. The accompanying cross-correlogram histograms (the columnwise sum of spike occurrence in perispike raster plots) revealed (close to time-lag zero) that, on average, cortical activity (CTX) led thalamic bursting (VPM1 and VPM2), i.e. cortical driving over thalamus was predominant in this behavioral state.

After convolving the spike trains with Eq. (2.1) using $1/T_s = 100$ Hz and $T_w = 50$ ms, causality analyses using segments of 1 (Fig. 10a), 2 (Fig. 10b) and 4 s (Fig. 10c) revealed consistent predominant flow of information

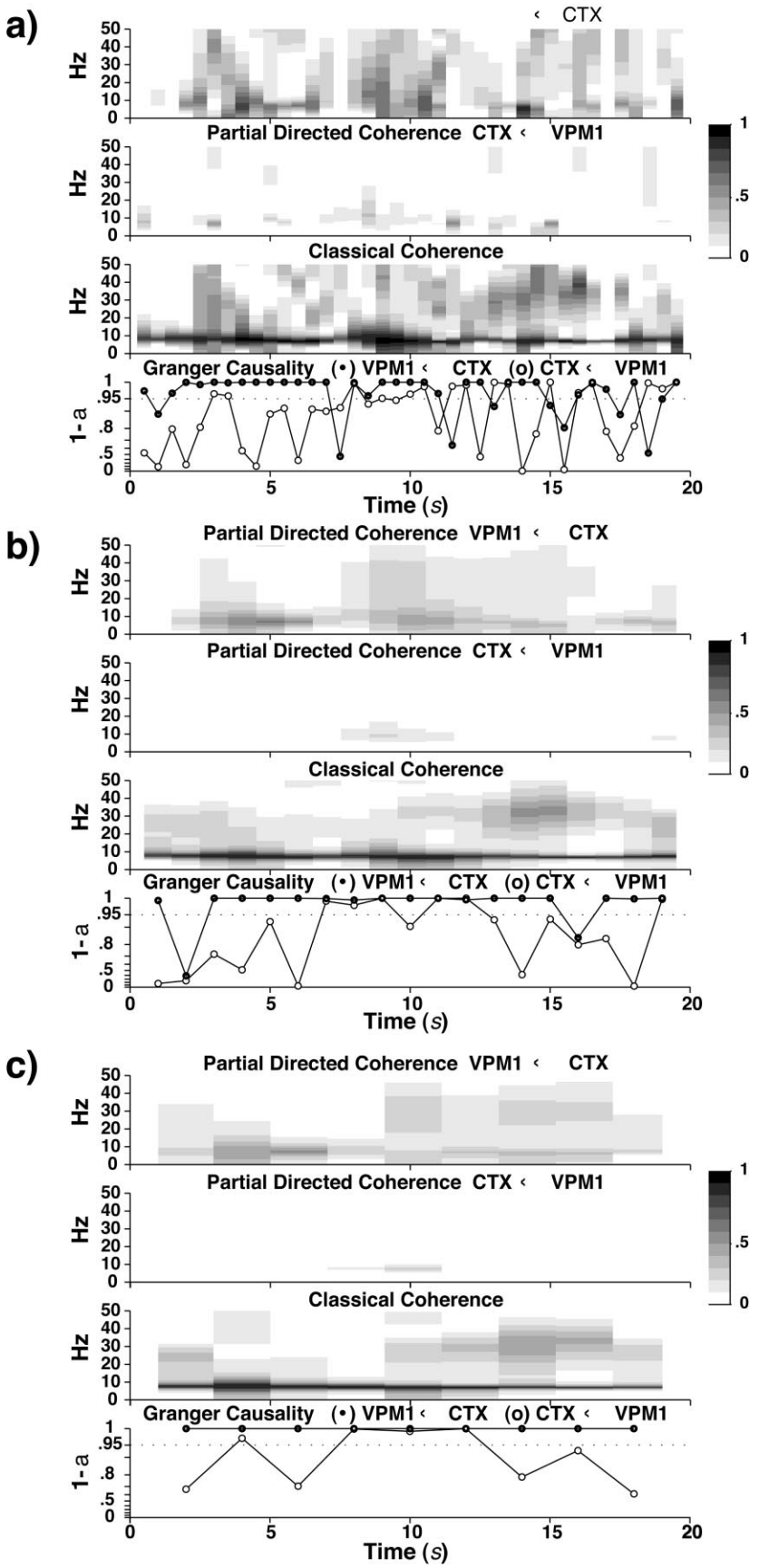

Fig. 10. Time-frequency representation of causality using segments of 1 s (a), 2 s (b) and 4 s (c) revealed consistent and predominant flow of information from cortex (CTX) to thalamus (VPM1) based on SCC (Remark 2). Throughout these time scales of analysis, use of the spectral criterion shows evidence of connection in the reverse direction (feedback) around the middle of the record where one can see light grey islets. This evidence is corroborated by the Granger test results for (b) and (c) (plots of the $1-\alpha = 95\%$ confidence level). Significant co-activation is apparent from the classical coherence plots of Fig. 10a throughout the record. The episodes of feedback from VPM1 to CTX are characterized by a subtle increase in the frequency which can be noted by inspecting the maximum of classical coherence in (a).

from cortex (CTX) to thalamus (VPM1) over these three time scales. In addition, consistent episodic functional connectivity in the opposite direction (light grey islets) was present in the middle of the record. Even though this conclusion was based on the use of SCC, which the previous examples showed to be the criterion of choice for oscillatory spike train data, GCT's results agreed with SCC over the 2 and 4 s long time scales of analysis. Furthermore, the feedback episodes coincided with an increased frequency of co-activation apparent from the classical coherence plot of Fig. 10a.

4. Conclusions

All of the available techniques that involve multivariate time series modelling, whether they use Granger causality explicitly (Baccalá et al., 1998; Baccalá and Sameshima, 1999) or not (Saito and Harashima, 1981; Franaszczuk et al., 1985; Wang and Takigawa, 1992; Franaszczuk et al., 1994; Takigawa et al., 1996; Kaminski et al., 1997), were originally developed for time sampled 'analog' signal processing — EEG and local field potentials. This paper's chief aim was to investigate whether one could use the best available multivariate time series modelling techniques directly for the analysis of spike train data. In this investigation we restricted our attention to rhythmic neuronal dynamic.

Examples 1 and 2 showed that partial directed coherence goes a step beyond correlation and classical coherence (which are also linear techniques) because of its ability to expose the direction of information flow, and because it highlights the presence of feedback between two or more simultaneously analyzed neural structures. In addition and perhaps more importantly, the method of partial directed coherence is capable of achieving high temporal resolution compared to correlative techniques.

Though further rigorous structural inference evaluation is required, the simulations of Examples 1 and 2 lend credence to the reality of the observed short-lived and frequency altering feedback from thalamus to cortex described in Example 3. Finally, within the dynamic regime of oscillatory neural spiking, SCC's performance was superior to GCT's and should be the criterion of choice specially when the processes involved are oscillatory and of the Poisson type.

Acknowledgements

We thank Erika Fanselow and Miguel Nicolelis for kindly providing the data of Example 3. Financial support: PRONEX, CNPq and FAPESP.

References

Aertsen AMHJ, Gerstein GL. Evaluation of neuronal connectivity: sensitivity of cross-correlation. Brain Res 1985;340:341–54.

Baccalá LA, Sameshima K. Directed Coherence: a tool for exploring functional interactions among brain structures. In: Nicolelis MAL, editor. Methods for Neural Ensemble Recordings. Boca Raton: CRC Press, 1998:179–92.

Baccalá LA, Sameshima K. Partial Directed Coherence a new concept in neural structure determination, IEEE Trans Biomed Eng 1999. Submitted.

Baccalá LA, Sameshima K, Ballester G, Valle AC, Timo-Iaria C. Studying the interaction between brain structures via directed coherence and Granger causality. App Sig Process 1998;5:40–8.

Bendat JS, Piersol AG. Random Data: Analysis and Measurement Procedures. 2nd ed. New York: John Wiley, 1986.

Bressler SL, Coppola R, Nakamura R. Episodic multiregional cortical coherence at multiple frequencies during visual task performance. Nature 1993;366:153–6.

Calford M, Tweedale R. Acute changes in cutaneous receptive-fields in primary somatosensory cortex after digit denervation in adult flying fox. J Neurophysiol 1991;65:178–87.

Donoghue J. Plasticity of adult sensorimotor representations. Curr Op Neurobiol 1995;5:749–54.

Duckrow RB, Spencer SS. Regional coherence and the transfer of ictal activity during seizure onset in the medial temporal lobe. Electroenceph Clin Neurophysiol 1992;82:415–22.

Eggermont JJ. The Correlative Brain: Theory and Experiment in Neural Interaction. Berlin: Springer-Verlag, 1990.

Eichenbaum HB, Davis JL. Neuronal Ensembles: Strategies for Recording and Decoding. New York: John Wiley, 1998.

Faggin B, Nguyen K, Nicolelis M. Immediate and simultaneous sensory reorganization at cortical and subcortical levels of the somatosensory system. Proc Nat Acad Sci USA 1997;94:9428–33.

Franaszczuk PJ, Bergey GK, Kaminski MJ. Analysis of mesial temporal seizure onset and propagation using the directed transfer function method. Electroenceph Clin Neurophysiol 1994;91:413–27.

Franaszczuk PJ, Blinowska KJ, Kowalczyk M. The application of parametric multichannel spectral estimates in the study of electrical brain activity. Biol Cybern 1985;51:239–47.

French AS, Holden AV. Alias-free sampling of neuronal spike trains. Kybernetik 1971;8:165–71.

Gochin PM, Miller EK, Gross CG, Gerstein GL. Functional interactions among neurons in inferior temporal cortex of the awake macaque. Exp Brain Res 1991;84:505–16.

Granger CWJ. Investigating causal relations by econometric models and cross-spectral methods. Econometrica 1969;37:424–38.

Kaminski M, Blinowska K, Szelenberger W. Topographic analysis of coherence and propagation of EEG activity during sleep and wakefulness. Electroenceph Clin Neurophysiol 1997;102:216–27.

Kaminski MJ, Blinowska KJ. A new method of the description of the information flow in the brain structures. Biol Cybern 1991;65:203–10.

Konig P, Engel AK, Singer W. Relation between oscillatory activity and long-range synchronization in cat visual-cortex. Proc Nat Acad Sci USA 1995;92:290–4.

Lutkepohl H. Introduction to Multiple Time Series Analysis. 2nd ed. Berlin: Springer-Verlag, 1993.

Marple Jr SL. Digital Spectral Analysis. Englewood Cliffs: Prentice Hall, 1987.

Merzenich MM, Nelson RJ, Stryker MP, Cynader MS, Schoppmann A, Zook JM. Somatosensory cortical map changes following digit amputation in adult monkeys. J Comp Neurol 1984;224:591–605.

Nicolelis MAL, Lin RCS, Woodward DJ, Chapin JK. Induction of immediate spatiotemporal changes in thalamic networks by peripheral block of ascending cutaneous information. Nature 1993;361:533–6.

Nicolelis MAL. Methods for Neural Ensemble Recordings. Boca Raton: CRC Press, 1998.

Nudo RJ, Plautz EJ, Milliken GW. Adaptive plasticity in primate motor cortex as a consequence of behavioral experience and neuronal injury. Semin Neurosci 1997;9:13–23.

Perkel D, Gerstein G, Moore G. Neuronal spike trains and stochastic point processes. II. Simultaneous spike trains. Biophys J 1967;7:419–40.

Priestley MB. Spectral Analysis and Time Series. London: Academic Press, 1981.

Recanzone GH, Merzenich MM, Jenkins WM, Grajski KA, Dinse HR. Topographic reorganization of the hand representation in cortical area 3b owl monkeys trained in a frequency-discrimination task. J Neurophysiol 1992;67:1031–56.

Saito Y, Harashima H. Tracking of information within multichannel EEG record-causal analysis in EEG. In: Yamaguchi N, Fujisawa K, editors. Recent Advances in EEG and EMG Data Processing. Amsterdam: Elsevier, 1981:133–46.

Schnider SM, Kwong RH, Lenz FA, Kwan HC. Detection of feedback in the central nervous system using system identification techniques. Biol Cybern 1989;60:203–12.

Schreiner CE, Mendelson J, Raggio MW, Brosch M, Krueger K. Temporal processing in cat primary auditory cortex. Acta Otolaryngol (suppl) 1997;532:54–60.

Takigawa M, Wang G, Kawasaki H, Fukuzako H. EEG analysis of epilepsy by directed coherence method-A data processing approach. Int J Psychophysiol 1996;21:65–73.

Wang G, Takigawa M. Directed coherence as a measure of interhemispheric correlation of EEG. Int J Psychophysiol 1992;13:119–28.

Wang X, Merzenich MM, Sameshima K, Jenkins WM. Remodelling of hand representation in adult cortex determined by timing of tactile stimulation. Nature 1995;378:71–5.

Wehmeier U, Dong D, Koch C, Van Essen D. Modeling the mammalian visual system. In: Koch C, Segev I, editors. Methods in Neuronal Modeling: From Synapses to Networks. Cambridge: MIT Press, 1989:335–59.